TWENTY FIRST EUROPEAN ROTORCRAFT FORUM

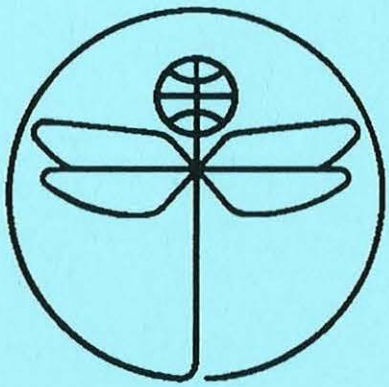

Paper No I.5

ROTOR AEROACOUSTICS AT HIGH-SPEED FORWARD FLIGHT USING A COUPLED FULL POTENTIAL/KIRCHHOFF METHOD

BY

C. Polacsek, M. Costes

Office National d'Etudes et de Recherches Aerospatiales
BP 72, 92322 Chatillion Cedex, France

August 30 - September 1, 1995
SAINT - PETERSBURG, RUSSIA

Paper nr.: I.5

Rotor Aeroacoustics at High-Speed Forward Flight Using a Coupled Full Potential/Kirchhoff Method.

C. Polacsek; M. Costes

TWENTY FIRST EUROPEAN ROTORCRAFT FORUM
August 30 - September 1, 1995 Saint-Petersburg, Russia

Rotor Aeroacoustics at High-Speed Forward Flight Using a coupled Full Potential/Kirchhoff Method

C. Polacsek, M. Costes
Office National d'Etudes et de Recherches Aérospatiales,
BP 72, 92322 Châtillon Cedex, France

ABSTRACT

A new acoustic code for HSI noise prediction (KARMA), based on the Kirchhoff formulation and coupled with a full potential rotor code (FP3D), is validated for forward flight applications and compared with experimental data. KARMA uses a fixed control surface method, which requires a post-processor to FP3D for transferring the CFD outputs from the rotating frame to the fixed frame. Several rectangular bladed model rotors are checked around delocalization conditions validated in wind tunnel. For each computed test case, experimental conditions and computation parameters are addressed. FP3D-KARMA calculations, tested on realistic configurations (lifting delocalized cases), give excellent results for rotor noise predictions.

NOTATIONS

c_0 :speed of sound
c :blade chord
d :distance between the source and the observer
$\vec{e}^i$:contravariant base vector, normal to ξ^j,ξ^k= cst
g^{ij} :contravariant metric tensor
M :wind tunnel flow Mach number
M_{at} :advancing tip Mach number
$\vec{n}$:normal vector to the Kirchhoff surface
n_i :normal components relative to a node of S_K
p :perturbed pressure
p' :acoustic pressure
R :rotor radius
R_K :Kirchhoff surface radius
S_K :Kirchhoff surface
t_0 :emission time
t :observer time
T :period of the acoustic signature (rotor blade revolution)
C_T/σ :non dimensional lift coefficient
x_i :observer coordinates in the fixed frame
y_i :source coordinates in the fixed frame
μ :advance ratio
Ψ :blade azimuth
ξ^i,ξ^j,ξ^k :curvilinear coordinates along aerodynamic grid lines

1. INTRODUCTION

High-speed helicopter forward flight produces transonic conditions on the advancing blade side. These are at the origin of the delocalization phenomenon, which generates intense impulsive noise radiation. High-speed impulsive noise (HSI noise) has been studied at ONERA for several years, by developing a two-step noise prediction method: near field Computational Fluid Dynamics (CFD) calculation and far field computation by an acoustic code using the CFD result as input data. The first approach was based on the Lighthill Acoustic Analogy (LAA) method, consisting in a volume integration of the Lighthill's stress tensor[1].

The main drawback with the LAA modeling is the requirement for a volume integration of the quadrupole terms. Various approximations have been proposed to bring the volume integral back to a surface integral in view of improved computational efficiency[2,1,3,4]. To get rid of these approximations, still keeping an integral formulation, an alternative is to use the Kirchhoff method. This approach integrates a known pressure field over a prescribed surface to build an acoustic wave front and propagate it to the far field.

Recent capability of CFD codes to compute accurate pressure field (including the capture of the shock waves) far enough from the rotor blade, has made this method applicable to HSI noise prediction.

Based on a linear Kirchhoff formulation, the KARMA (Kirchhoff Advancing Rotor Method for Acoustics) code has been developed. KARMA computes rotor noise as an integral on a surface (cylinder), the axis of which coincides with the rotor axis. The inputs are the acoustic pressure and its normal gradient (provided by a CFD code) on the control surface. The suitability of a fixed (referenced to the helicopter frame) Kirchhoff surface formulation instead of a rotating (linked to the rotor blade) one, for delocalized case prediction, has been discussed in a recent paper[5].

The input data to KARMA (using the fixed Kirchhoff surface method) are provided by the Full Potential code (FP3D)[6] of ONERA. FP3D and KARMA features are briefly described and the paper focuses on applications relative to several forward flight rotor tests in wind tunnels:

- two non-lifting delocalized and non-delocalized cases of ONERA model rotors in the S2-Chalais wind tunnel[7], already presented in[5];
- a delocalized lifting case relative to the Helinoise BO-105 rotor tests in the DNW wind tunnel[8];
- a strongly delocalized lifting case relative to the 7A rotor tested in the S1-Modane wind tunnel[9].

For these calculations, computation parameters including mesh spacing, integration domain and radial position of the control surface are addressed.

Results presented in the paper are computed blade pressure (FP3D) and acoustic signatures (FP3D-KARMA), both correlated with experiment.

2. FIXED KIRCHHOFF SURFACE METHOD

2.1. Kirchhoff Formulation

KARMA calculates the acoustic pressure according to Kirchhoff formulation as:

$$p'(x,t) = \int_0^T \int_{S_k} \frac{1}{4\pi d}\left[-M^2\frac{\partial p}{\partial n_1} + \frac{\partial p}{\partial n} - \beta^2\frac{p}{d^2}n_i(x_i-y_i) - \frac{1}{c_0}\left(\frac{n_i(x_i-y_i)}{d} + M n_1\right)\frac{dp}{dt_0}\right] dS\, dt_0$$

This equation, already discussed in[5], is an extension to forward flight of the standard form currently used in hover, with the Kirchhoff surface, S_K, fixed in the wind tunnel (or helicopter) frame. In KARMA, S_K is a fixed cylinder surrounding the rotor, open at the top and bottom bases.The input data required on this cylinder for the calculation of the Kirchhoff integral are the pressure and its gradient (the pressure derivative is numerically obtained from pressure stored at each time step). These data are provided by the FP3D code.

2.2. Interpolation of CFD Input Data

The acoustic code includes a post-processor to FP3D, to transfer CFD output data from the rotating frame, for which grid points are not equally spaced in azimuth, to the nodes of the fixed grid of the control surface, for which a constant azimuthal spacing is used. This is done by using a 2D bilinear interpolation program.

3. FP3D AND KARMA FEATURES

3.1. FP3D Code

The FP3D code solves the Unsteady Full-Potential equation for an isolated blade, using an implicit finite-difference algorithm in the relative frame linked to the blade. The space discretization

uses a second order centered finite-volume-like scheme, with upwinding in the supersonic zones using the Engquist-Osher flux biasing. Nonreflecting boundary conditions are applied in the far-field, while a transpiration condition is imposed on the blade in order to simulate the full rotor system and its wake. Inflow conditions are given by the R85/METAR code[10], which solves the blade dynamics coupled to the rotor and wake aerodynamics using a lifting line analysis on the blade and vortex lattices for the wake. Time discretization in FP3D is obtained from first-order fluxes and density linearization; these linearizations can be converged at each time-step using Newton iterations, but for the present calculations, a simple linearization was applied.

The grid used in the present calculations are C-H grids, each C-grid surface lying on a cylinder centered at the rotor hub. A typical grid density for the aerodynamic calculations consists of 141 x 31 x 21 points.

3.2. FP3D Output Data and Adaptations for KARMA

The aerodynamic data needed by the Kirchhoff analysis are the pressure and pressure gradients on the Kirchhoff surface. The pressure is a direct output from FP3D. For the pressure gradients, previous calculations were performed by an external interface between FP3D and KARMA, from the storage in FP3D of the pressure field on three cylinder surfaces surrounding the Kirchhoff surface. To improve the method efficiency and accuracy, a direct computation of the pressure gradients in the FP3D code was added, using tensor analysis. The Kirchhoff surface lies on a selected C-grid surface, sufficiently far from the blade tip such that nonlinear effects are accounted for. The normal vector to this surface is then:

$$\vec{n} = \frac{\vec{e}^{\,i}}{\sqrt{g^{ii}}}$$

and since the pressure gradient is equal to:

$$\vec{\nabla} p = \frac{\partial p}{\partial \xi^j}\,\vec{e}^{\,j}$$

the normal pressure gradient is computed as:

$$\frac{\partial p}{\partial n} = \frac{1}{\sqrt{g^{ii}}}\left(g^{ij}\,\frac{\partial p}{\partial \xi^j}\right)$$

and the streamwise pressure gradient is computed as:

$$\frac{\partial p}{\partial n_l} = \frac{\partial p}{\partial x}\sin(\psi) + \frac{\partial p}{\partial y}\cos(\psi)$$

In all these formulae, the gradients are computed using second-order finite-differences, and the projections use the metric quantities computed from a finite-volume interpretation.

Practically, in order to reduce the size of the data files, the numerical Kirchhoff integration is limited between azimuths 15 degrees to 255 degrees, assuming that out of this domain, the acoustic sources can be neglected.

3.3. KARMA Code Information

KARMA computes the acoustic pressure time histories for one or several observers (multi-observer version) corresponding to microphone locations in the wind tunnel frame.

The azimuthal spacing of the acoustic grid (equal to the azimuthal step storage of FP3D output data) roughly corresponds to the sampling rate of the experimental data. The vertical spacing is chosen to correspond to the aerodynamic one at the trailing edge.

KARMA CPU time, including FP3D post-processor, is about 30 min on a CRAY YMP for lifting cases.

4. FORWARD FLIGHT APPLICATIONS

4.1. Non-lifting Cases

4.1.1. Experimental conditions

The first forward flight computations using FP3D-KARMA codes have been applied to the ONERA S2-Chalais wind tunnel tests[7] on a rectangular two-bladed model rotor (Fig. 1). The rotor is stiff, untwisted, with symmetrical airfoils, and the lift is set to zero. The rotor diameter is 1.5 meters and the blade aspect ratio is 5.36. The observer position corresponds to a microphone located at 3 meters from the rotor hub, in the rotor plane and in the advancing direction. During the tests, the walls of the closed test section were covered with acoustic lining.

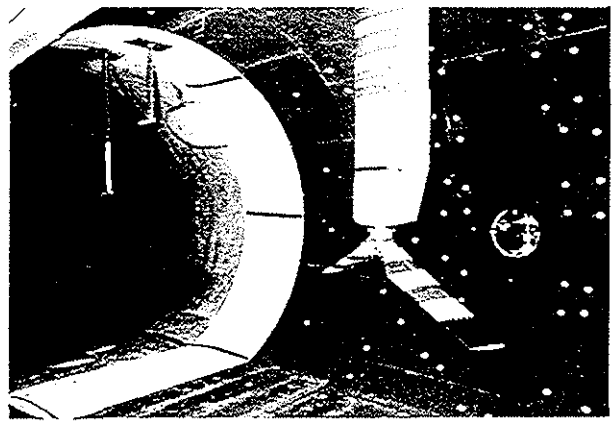

Fig. 1 - Acoustic test set-up in the S2-Chalais wind tunnel on a high-speed non-lifting rotor.

Two computational test cases are presented: a non-delocalized case at $M_{at} = 0.869$ ($\mu = 0.413$), and a case at the beginning of delocalization, at $M_{at} = 0.9$ ($\mu = 0.4$). The experimental acoustic signatures and spectra relative to these configurations are shown in Fig. 2. The experimental acoustic sampling rate is 1024 points per rotor revolution.

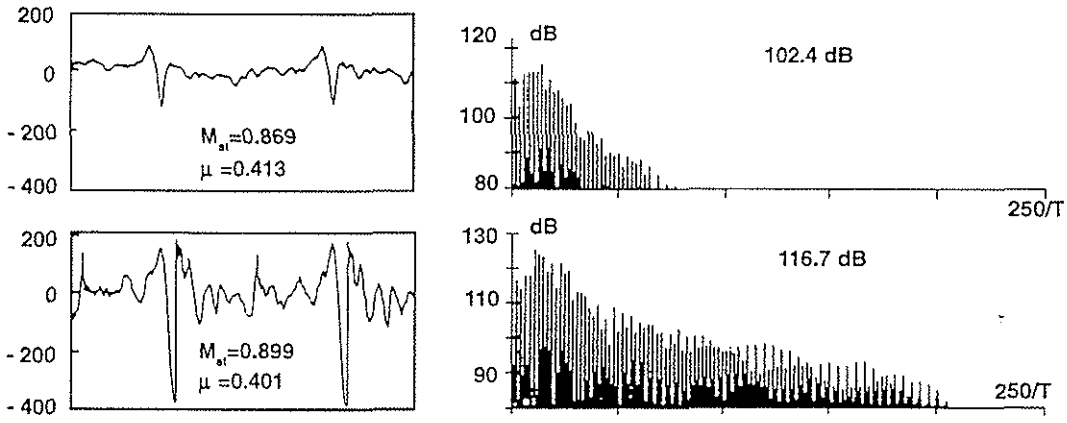

Fig. 2 - Experimental acoustic results (signature and spectrum) relative to the non-lifting computed test cases.

4.1.2. Computational Parameters

The Kirchhoff surface, located at 1,27 R[5], is limited to a half cylinder (non lifting calculations). The acoustic grid extends from -3.5 c to +3.5 c in the chordwise direction with a regular azimuthal spacing equal to 0.3 degree (corresponding to a sampling rate of 1200 points per rev.).

4.1.3. Theory and Experiment Correlation

KARMA predicted pressure time histories are compared to experiment in Fig. 3a ($M_{at} = 0.869$) and Fig. 3b ($M_{at} = 0.9$).

For the non-delocalized case (Fig. 3a), the correlation is quite good except for the bounds before and after the main pulse (the recompression, in particular, is slightly overpredicted). Main differences can be due to residual acoustic wall reflections which affect the experiment, and also, for theory, to the finite difference methodology in FP3D, which is not well-adapted to the C-grid singularity present at the leading-edge line off the tip.

For the second case, correlation between both signatures is excellent.

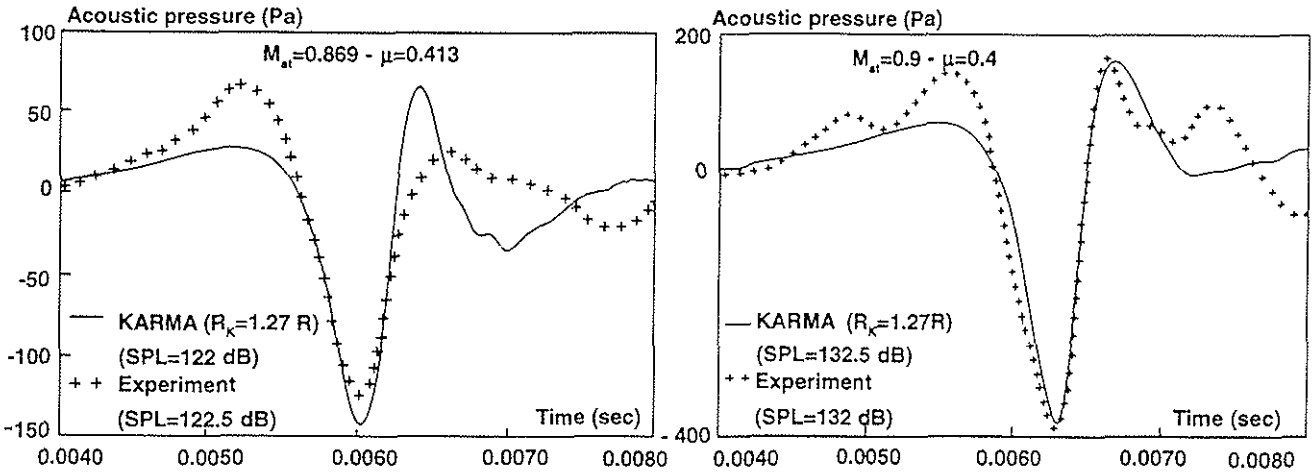

Fig. 3 - Comparison between FP3D-KARMA predicted acoustic pressure time histories and experiment, relative to a rectangular bladed model rotor in non-lifting forward flight.

For both cases, the intensity and the slopes of the main pulse are well predicted, so that the theoretical and experimental Sound Pressure Levels (SPL), indicated in the figure, are very close together.

4.2. Lifting Case under Delocalization Conditions

4.2.1. Experimental conditions

The BO-105 model rotor has been tested in the DNW (Fig. 4) within the HELINOISE Aeroacoustic Program[8]. The four-bladed rotor is 4 meters diameter, rectangular, linearly twisted, and hingeless. The blade aspect ratio is 16.53.

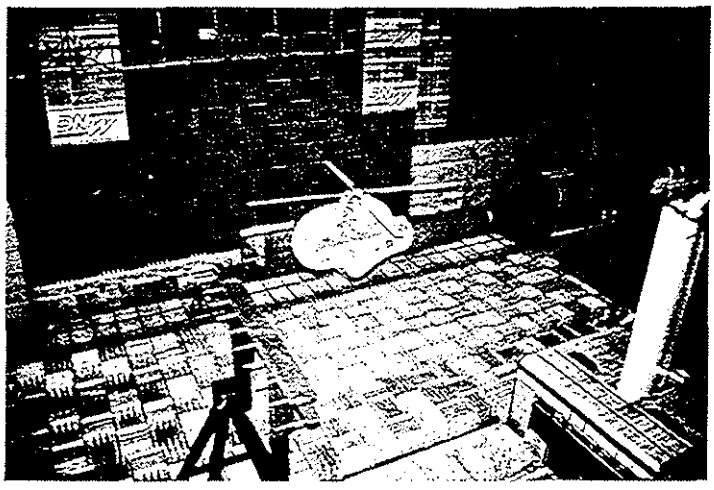

Fig. 4 - Experimental set-up installed in the DNW open test section for the HELINOISE program.

The acoustic data used for HSI noise predictions have been provided by measurements from a microphone array (Fig. 5) located at 2.3 meters under the rotor plane and 5.5 meters away from the rotor axis, in the upstream direction. The three microphones (M6, M8, M11) used for theory and experiment comparisons presented here are indicated in Figure 5.

The computed case corresponds to the highest speed condition: $M_{at} = 0.9$ and $\mu = 0.337$. This is a forward flight lifting case, with a non dimensional lift C_T/σ equal to 12.

The experimental acoustic sampling rate is 2048 points per rev.

4.2.2. Computational Parameters

The Kirchhoff surface radius is kept roughly the same (R_K = 1.22 R), the values of the advancing tip Mach number being very close from those of the previous test cases relative to S2-Chalais. The azimuthal spacing should have been decreased to roughly correspond to the experimental sampling rate (2048 per rev.), but to limit the size of input data files (and assuming it does no affect the calculation), the azimuthal step used in section 4.1 was kept. On the other hand, the acoustic mesh is extended up from ± 3.5 to ± 8 c in the chordwise direction, because the aspect ratio of the BO-105 rotor is much larger than the S2 Chalais rotor.

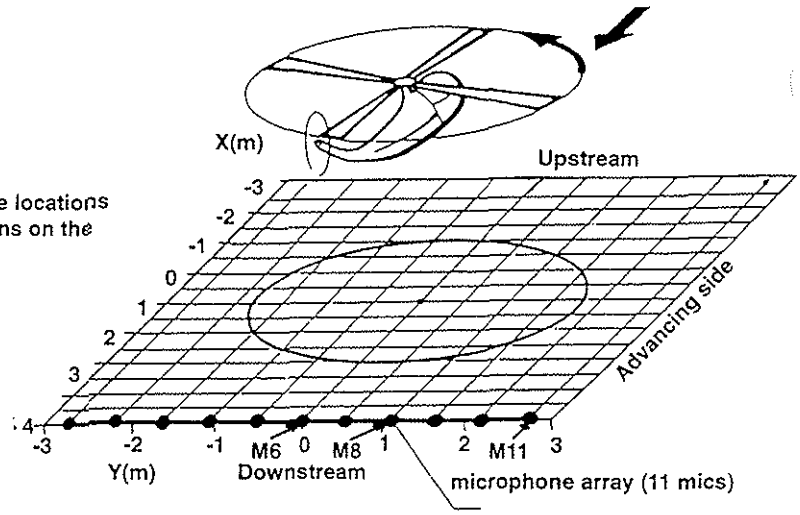

Fig. 5 - Acoustic measuring plane and microphone locations in the DNW relative to FP3D-KARMA computations on the BO-105 model rotor.

4.2.3. Theory and Experiment Correlation

Blade pressure coefficients

The aerodynamic calculation with FP3D was made using computed R85/METAR inflow conditions. With R85/METAR, the BO-105 rotor was trimmed to the experimental condition (zero flapping) taking into account the blade elastic deformations. The inflow conditions given to FP3D therefore include the blade motion and deformation, and the wake influence from which the near wake has been removed since it is already computed in FP3D. In order to simulate this hingeless rotor in R85/METAR, equivalent hinge positions were defined.

The pressure distribution for the three instrumented sections is shown respectively in Figures 6a, 6b and 6c, for 60°, 90°and 120° azimuth. The correlation with experiment is disappointing, showing that the blade angle of attack is underestimated before $\Psi = 90°$ and overestimated after $\Psi = 90°$.This is particularly noticeable for the most inboard section, while the outboard one gives better results. The reason for this discrepancy between calculation and experiment is difficult to explain, since the R85/METAR trim conditions fit the experimental ones, in terms of pitch angle as well as consumed power. Dynamics (in particular torsional) problems are suspected for this soft-in-torsion hingeless rotor. However, the computation-experiment correlation was estimated sufficiently reasonable to perform a KARMA noise calculation.

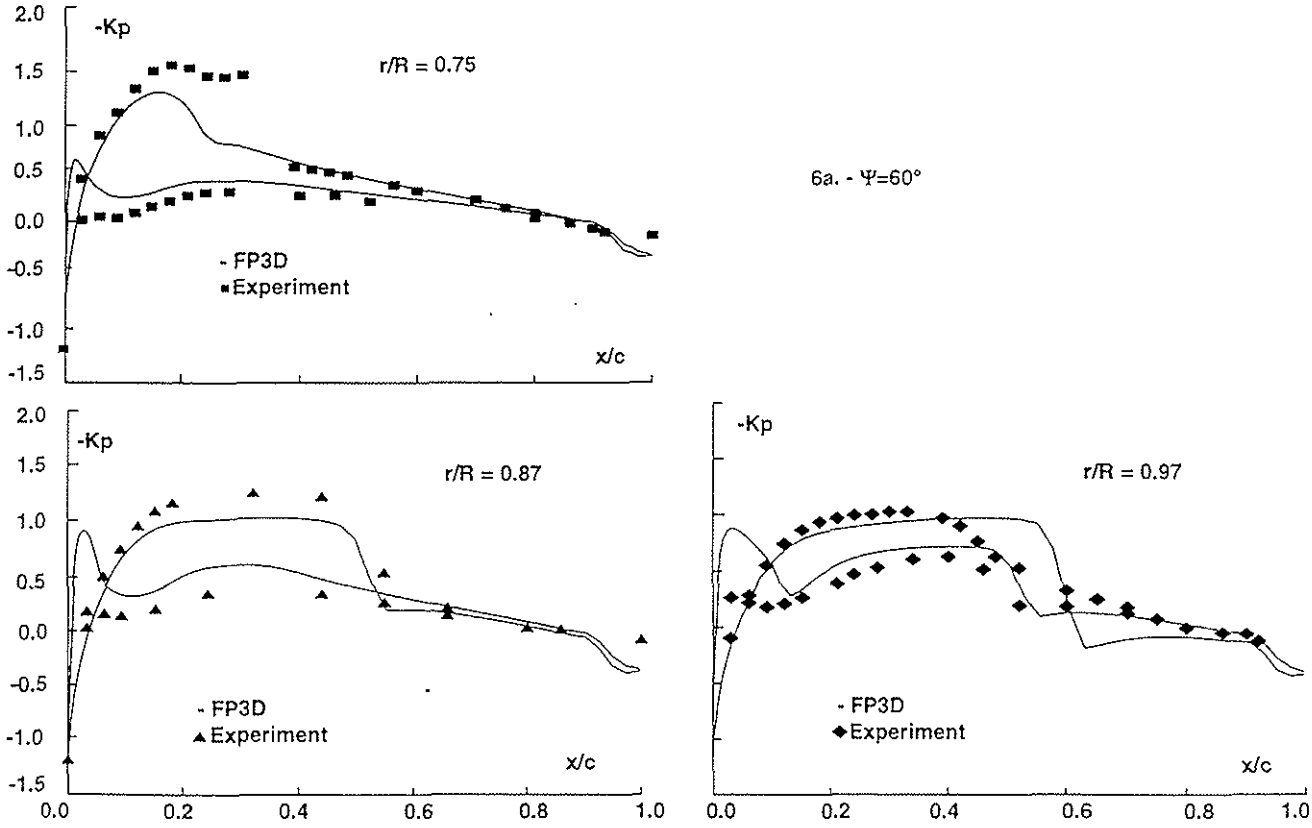

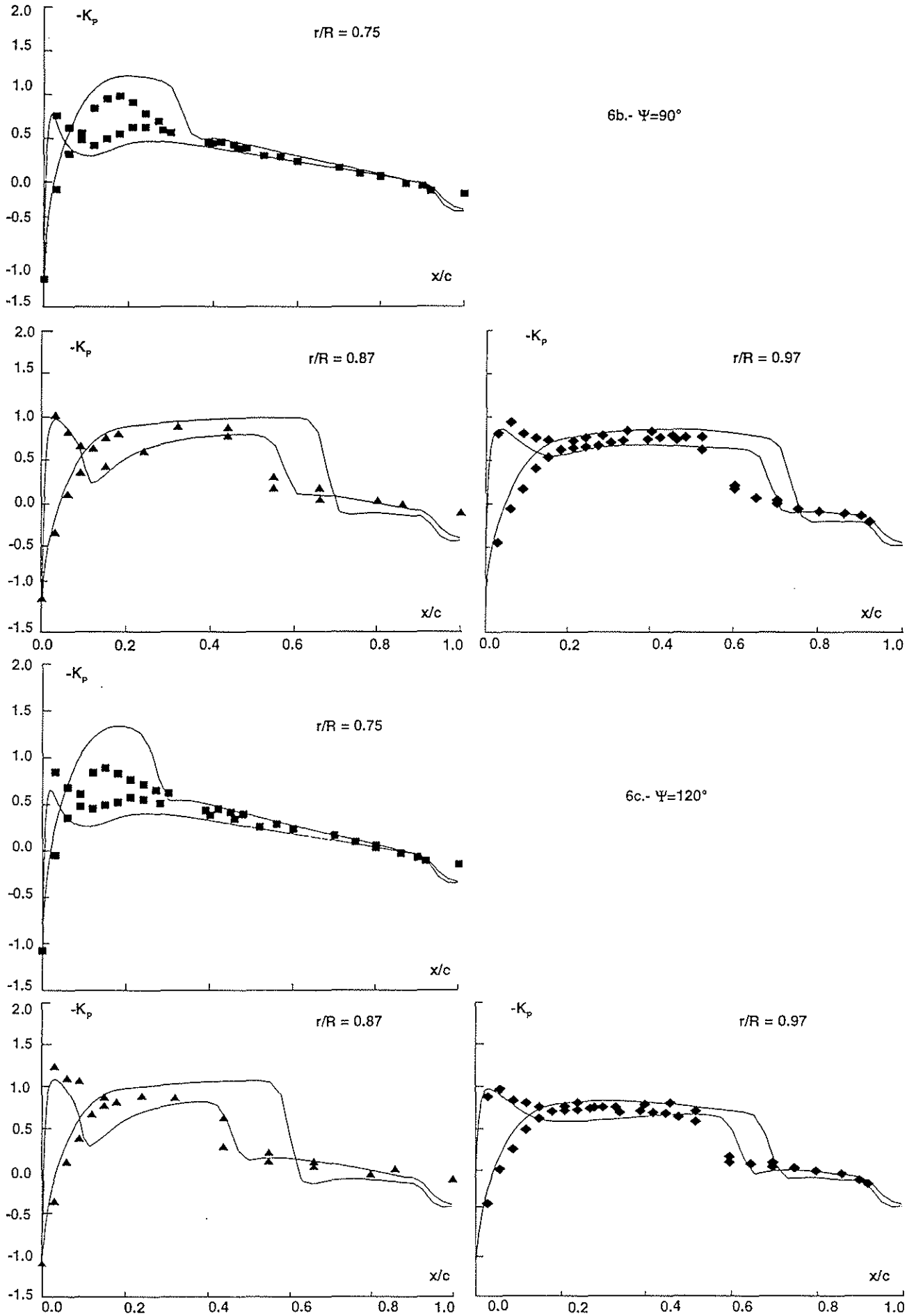

Fig.6- Comparaisons between computed (FP3D) and experimental local blade pressure distributions for a delocalized lifting forward- flight case relative to the BO- 105 model rotor.

Acoustic Signatures

Acoustic signature comparisons relative to the three microphones are shown in Figures 7a, 7b and 7c. Basic shapes and negative amplitudes are correctly predicted, but the acoustic pressure relative to the compressions before and after the main pulse are overestimated. This is a direct consequence of local erroneous lift estimation on the advancing blade side by FP3D, due to the fact that predicted angles of attack for some radial locations are more important than the experimental ones. As previously mentioned, the BO-105 rotor trim is very difficult to simulate due to high torsion deformations, and since the blade is non articulated. These blade deformations effects might also be at the origin of typical time fluctuations occurring after the main pulse of the experimental acoustic signature relative to Mic. 11 (Fig. 7c).

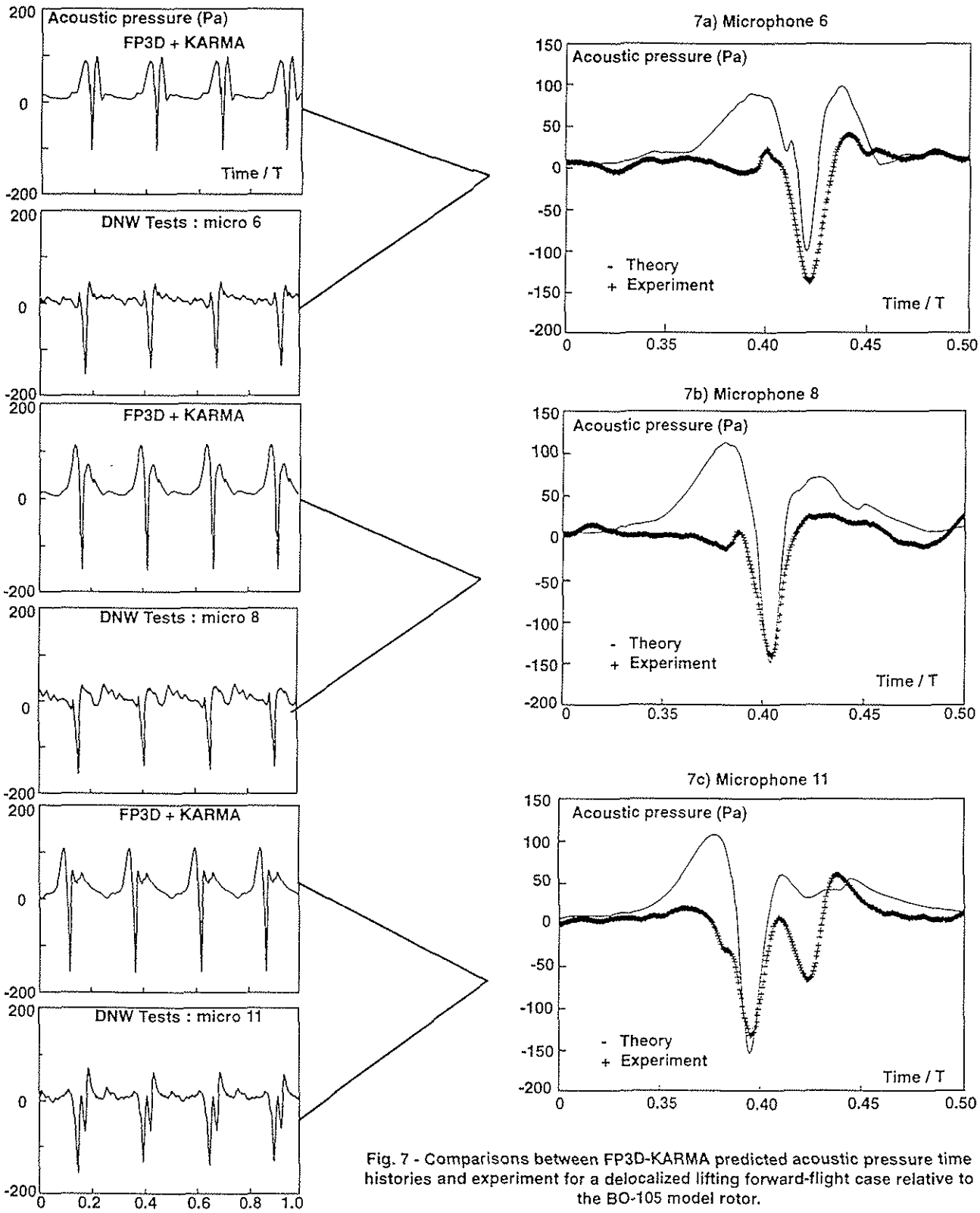

Fig. 7 - Comparisons between FP3D-KARMA predicted acoustic pressure time histories and experiment for a delocalized lifting forward-flight case relative to the BO-105 model rotor.

4.3. Strongly Delocalized Lifting Case

4.3.1. Experimental Conditions

HSI helicopter rotor noise measurements have been performed in 1990 in the ONERA S1-Modane wind tunnel fitted with acoustic lining (Fig. 8). KARMA is tested on a strongly delocalized lifting case relative to the 7A rectangular four-bladed model rotor, which is 2.1 meters radius. The blade is linearly twisted with non symmetrical airfoils, and the blade aspect ratio is 15.

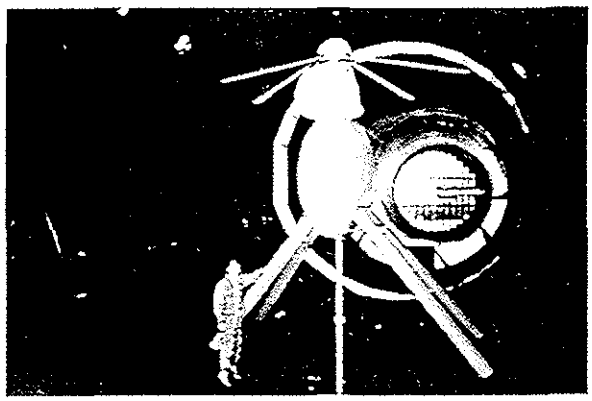

Fig. 8 -Helicopter rotor test set-up in S1-MA wind tunnel with acoustic lining on the wall.

The test parameters are: $M_{at} = 0.936$, $\mu = 0.45$, $C_T/\sigma = 12.5$. The experimental sampling rate is 1024 points per rev. Theory and experiment are correlated for three microphone locations shown in Figure 9. These positions belong to the noisiest far field regions, where radiated HSI rotor noise is very intense.

4.3.2. Computational parameters

As compared to section 4.2, the Kirchhoff surface radius is drawn back to 1.19 R, due to the fact that the sonic cylinder is very close to the rotor (1.07 R), and the azimuthal spacing is unchanged. Since the aspect ratio of the BO-105 and the one of the 7A rotor are quite the same, the acoustic mesh extent in the chordwise direction is not modified (± 8c)

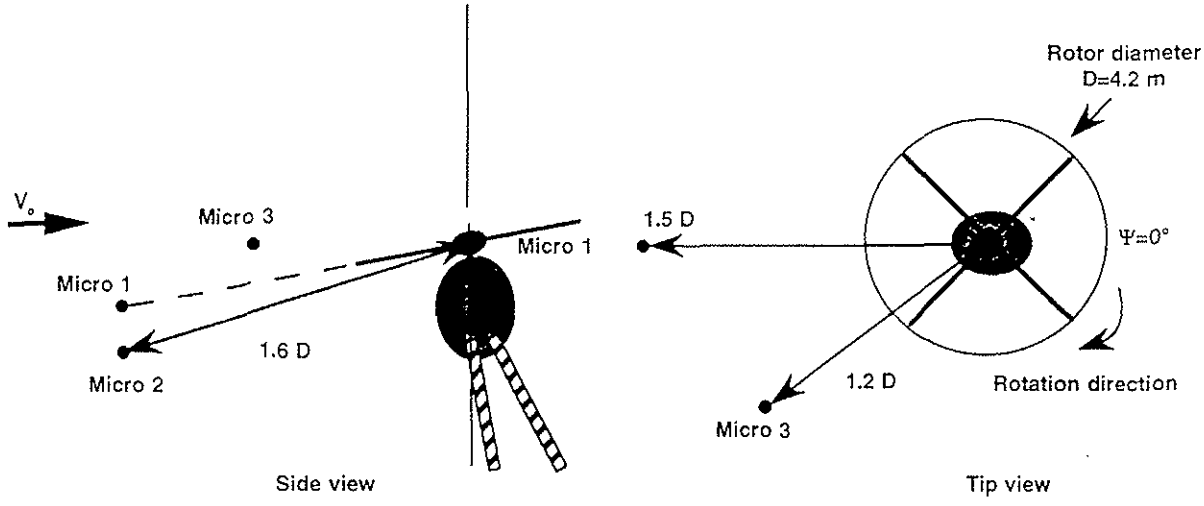

Fig. 9 -Microphone locations in S1-MA used for KARMA computations on the 7A model rotor.

4.3.3. Theory and Experiment Correlation

Blade pressure coefficients

As for the BO-105 rotor, FP3D uses R85/METAR trimmed inflow conditions. The correlation between the computed blade pressure and the experiment (Fig. 10) is much better here (only 90 degrees azimuth is shown), although the shocks intensity is overestimated on the blade. However, the lift distribution on the blade seems to be in good agreement with experiment.

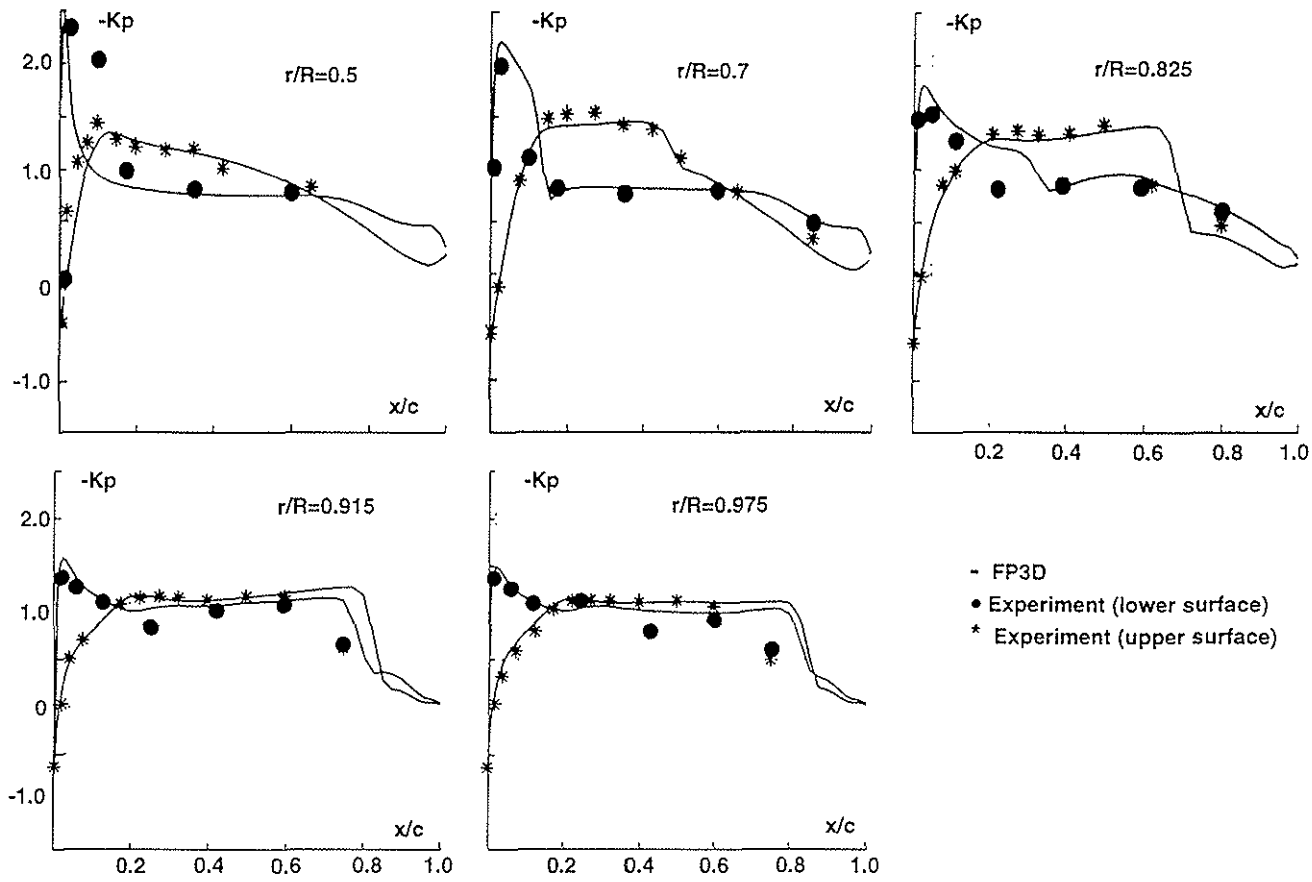

Fig.10 - Comparisons between computed (FP3D) and experimental local blade pressure distributions for a strong delocalized lifting forward-flight case relative to the 7A model rotor.

Acoustic signatures

Acoustic pressure time histories provided by FP3D-KARMA are compared to experiment in Figures 11a, 11b and 11c, respectively for each microphone. For the three cases, in spite of the difficulty of the calculation due to high transonic effects, correlation between theory and experiment is very good, thanks to the accuracy of input data (see above). Negative peak pressures and recompression slopes are correctly predicted. The only differences concern the high frequency extent of the signatures (see the experimental recompression peak amplitude) which is slightly underpredicted by the calculation (if we assume the experiment to be perfectly correct). This can be due to the methodology used in FP3D where the potential field has been computed at the nodes of the aerodynamic mesh. Underway calculations using a new methodology, which solves the potential equation at the center of the cells, are expected to give some significative improvement with respect to the capture of high frequency time fluctuations. Anyway, present results relative to this realistic test case are quite satisfactory for rotor noise applications.

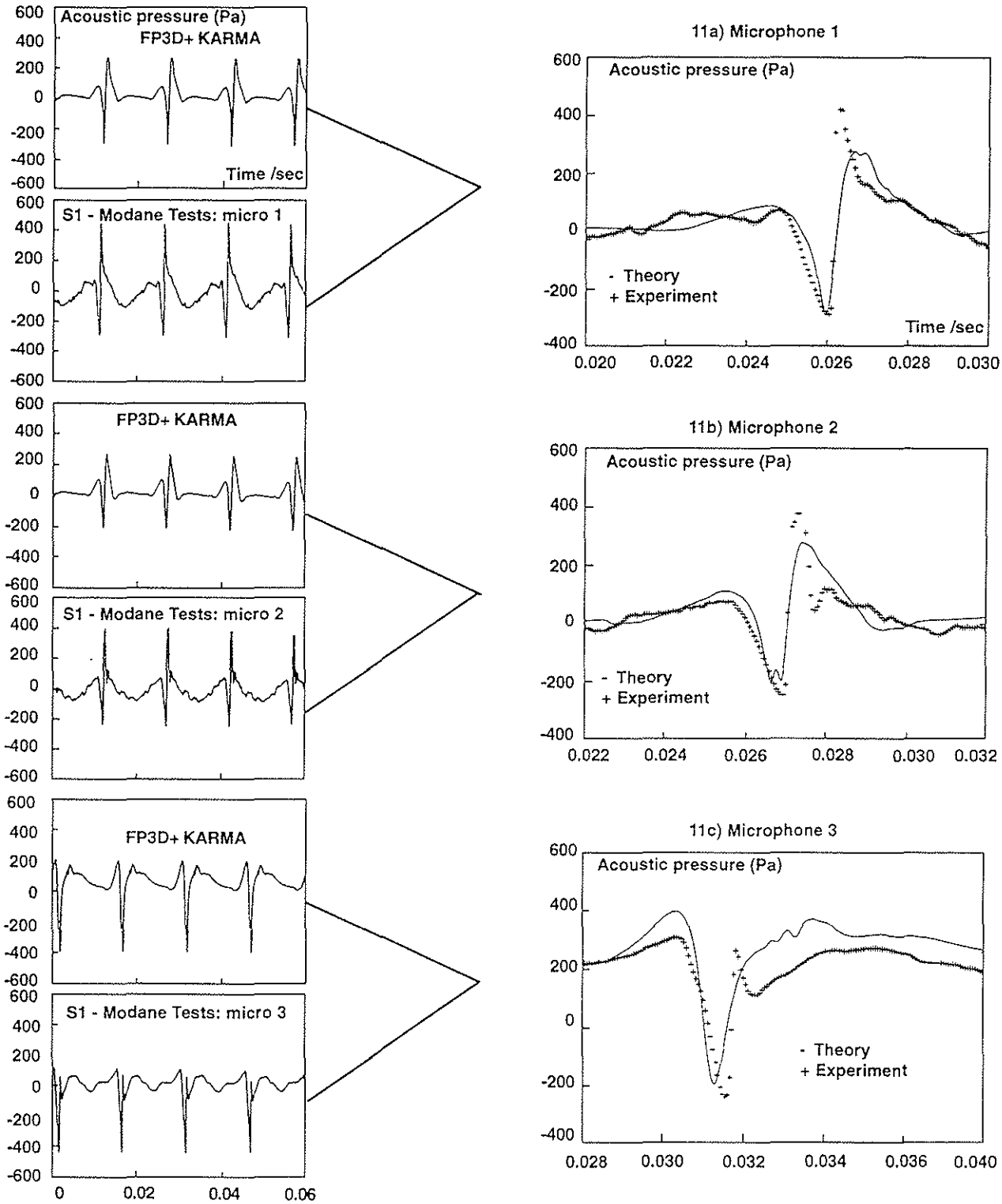

Fig.11- Comparaisons between computed FP3D-KARMA predicted acoustic pressure time histories and experiment for a strong delocalized case in forward- flight relative to the 7A model rotor.

5. CONCLUSION

The Kirchhoff method (KARMA code), coupled with a full potential rotor code (FP3D code), has been applied with success on forward flight configurations, including realistic delocalized lifting cases. Correlations with experiment are very good, except for the BO-105 model rotor, probably because of rotor trim simulation errors. Underway adaptations of FP3D methodology should improve the predictions. These results relative to lifting rotor cases, never yet addressed by the HSI rotor noise research community, constitute an additional evidence of the suitability of the Kirchhoff approach.

ACKNOWLEDGEMENTS

This work was funded by the French Ministry of Defence (Service Technique des Programmes Aéronautiques). The BO-105 rotor calculations were also partially funded by the European Union under Brite Euram contract HELISHAPE.

REFERENCES

1. J. Prieur. Calculation of Transonic Rotor Noise using a Frequency Domain Formulation. AIAA Journal, Vol. 26 (2), February 1988, pp. 156-162.

2. F.H. Schmitz, Y.H.Yu. Transonic Rotor Noise - Theoretical and Experimental Comparisons. Vertica, Vol. 5 (1), 1981, pp. 55-74.

3. F. Farassat, H. Tadghighi. Can Shock Waves on Helicopter Rotors Generate Noise ? A study of Quadrupole Sources. 46th AHS Forum, Washington D.C., May 1990.

4. K.J. Schultz, D. Lohmann, J.A. Lieser, K.D. Pahlke. Aeroacoustic Calculation of Helicopter Rotors at DLR. 75th Fluid Dynamics Panel Meeting and Symposium on Aerodynamics and Aeroacoustics of Rotorcraft, Berlin, Germany, October 1994.

5. C. Polacsek, J. Prieur. High-Speed Impulsive Noise Computations in Hover and Forward Flight using a Kirchhoff Formulation. 16th AIAA Aeroacoustics Conference, Munich, Germany, June 1995.

6. P. Beaumier, M. Costes, R. Gaveriaux. Comparison between FP3D Full Potential Calculations and S1 Modane Wind Tunnel Tests Results on Advanced Fully Instrumented Rotors. 19th ERF, Cernobbio, Italy, September 1993.

7. J. Prieur. Experimental Study of High-Speed Impulsive Rotor Noise in a Wind Tunnel. 16th ERF, Glasgow, Scotland, September 1990.

8. W.R. Splettstoesser. Experimental Results of the European HELINOISE Aeroacoustic Rotor Test in the DNW. 19th ERF, Cernobbio, Italy, September 1993.

9. C. Polacsek, P. Lafon. High-Speed Impulsive Noise and Aerodynamic Results for Rectangular and Swept Rotor Blade Tip Tests in S1-Modane Wind Tunnel. 17th ERF, Berlin, Germany, September 1991.

10. G. Arnaud, P. Beaumier. Validation of R85/METAR on the Puma RAE Flight Tests. 18th European Rotorcraft Forum, Avignon, France, September 1992.